

Single-disk and double-disk viscous micropumps

Danny Blanchard, Phil Ligrani*, Bruce Gale

University of Utah, Department of Mechanical Engineering, 50 South Central Campus Drive, Rm. 2110 Salt Lake City, UT 84112, USA

Received 6 October 2004; received in revised form 25 March 2005; accepted 26 March 2005

Available online 29 June 2005

Abstract

The development and testing of two versions of a novel micropump are described: (i) the single-disk viscous pump and (ii) the double-disk viscous pump. The rotational movement of the disk(s) induces viscous stresses on the fluid that forces the fluid from an inlet channel, and then, through the pumping volume above the single disk, or between the two disks. A wiper acts to “wipe” the fluid from the disk(s) toward the outlet channel. The fluid flow through the double-disk pump is visualized using a red Rhodamine dye that is injected into the fluid passage upstream of the pumping volume. These visualizations provide information on the relative importance of viscous forces, centrifugal forces, and static pressure variations. The maximum flow rates and pressure rises are 1.0 ml/min, 643 Pa, and 2.1 ml/min 1.19 kPa for the single-disk and double-disk pumps, respectively, for a rotational speed of 5000 rpm, a disk diameter of 2.38 mm, and a gap height of 103 μm , and supplied power to the motor of 7 W. The disk pumps are fabricated using precision machining techniques employed on a lathe and milling machine. Advantages of the viscous disk pumps include: simplicity of design, planar structure, continuous flow, well controlled flow rate, and, if desired, the ability to augment mixing in the fluid.

© 2005 Elsevier B.V. All rights reserved.

Keywords: Micropump; Rotary; Disk; Viscous; Visualization; Pump

1. Introduction

The area of microfluidics is developing with many new sensors, separation devices, drug delivery systems, and other small-scale and micro-scale fluidic devices. For many of these devices there is a need to circulate or move fluid through macroscale and microscale channels. A variety of micropumps are available to meet this need, generally to fulfill specific applications [1]. These include membrane pumps [2–8] (both without check valves [2–4] and with check valves [5–8]), electrohydrodynamic (EHD) pumps [9–11], electrokinetic (EK) pumps [12,13], rotary pumps [14–18], peristaltic pumps [19–21], bubble based pumps [22,23], and several other types of pumps [24–26]. Non-mechanical pumps like the electrohydrodynamic and electrokinetic pumps do not have moving parts, which increases reliability. However, such devices are generally limited by low flow rate and pressure rise capabilities, the applications of the pump,

the working fluids that can be pumped, and high supply voltage requirements [1]. Mechanical pumps, like rotary pumps, peristaltic pumps, and membrane pumps, have a wide variety of possible working fluids and applications. However, such mechanical micropumps are believed to be feasible only when they are greater than a certain size [1], due to the large viscous forces of the fluid for small pump geometries. At very small scales, viscous forces are significant, which result in large pressure drops over small streamwise distances [27]. One motivation of the present effort is to develop miniature pumps that produce well controlled, constant flow rates by employing these large viscous forces to produce a pumping action.

Several pumps are developed that employ the viscous shear to produce a pumping action. Kilani et al. [15] presents one such pump called a spiral pump. This pump uses one spinning disk rotating over a spiral channel to produce a pumping effect. Only results from a macroscale version of this pump have been published thus far. The small-scale version of this pump may be complex to fabricate. Sen et al. [16] present a pump that uses a shaft, whose axis is perpendicular to the

* Corresponding author. Tel.: +1 801 581 4240; fax: +1 801 585 9826.
E-mail address: ligrani@mech.utah.edu (P. Ligrani).

Nomenclature	
A	stagnation point on inlet wiper face
B	stagnation point on outlet wiper face
g	gravitational constant
h	vertical height between the top of the fluid reservoir and top of the water tank
P	power supplied to motor (W)
ΔP_{\max}	maximum pressure rise across the disk pumps
Q	volumetric flow rate (ml/min)
r	radial direction
z	z -direction
<i>Greek letters</i>	
ρ	fluid density
Ω	rotational speed (rpm)
θ	circumferential direction

flow direction, and is positioned eccentrically in the channel. The difference in viscous shear between the shaft and the two channel walls produces a net pumping effect. This pump is easy to fabricate, but has limited flow rates and pressure rise capabilities.

In the present paper, a new set of micropumps are described, called the double-disk and single-disk viscous pumps, to achieve flow rates and pressure rises greater than 1.0 ml/min and 1.0 kPa, respectively, while maintaining simplicity and ease of manufacturing. The present disk pumps are unique because they use the viscous stress to produce a pumping effect by employing one or two disks and a wiper to force fluid through a passage [28,29]. The two axially collinear disks, or the disk and the top pump housing, are separated by a small gap. The wiper is situated between the spinning disk(s). Fig. 1 shows a cross-sectional view of the disk pumps. The spinning of the disk(s) cause a net movement of fluid due to the viscosity of the fluid, and the transfer of momentum

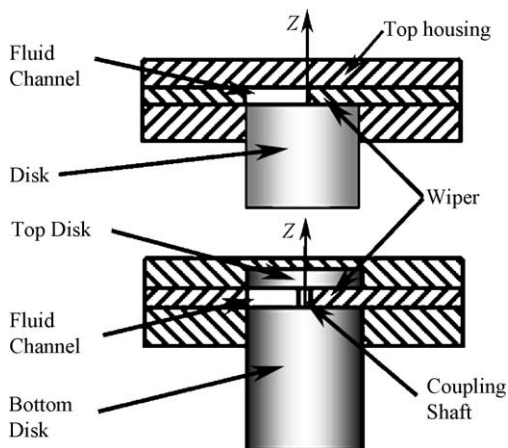


Fig. 1. Cross-sectional view of the single-disk and double-disk pumps.

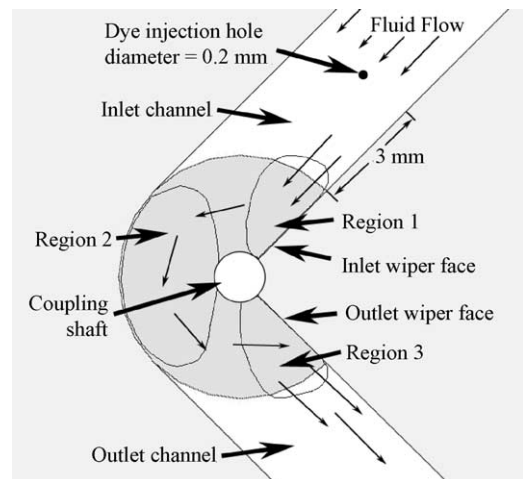


Fig. 2. Top view of the single-disk pump. Arrows indicate flow direction. Disk rotates counterclockwise.

from the disks to the fluid. The wiper acts to “wipe” the fluid off the disk(s), and to direct the fluid into the outlet channel. Fig. 2 shows the movement of the fluid through the single-disk pump as indicated by the small arrows. The advantages of this micropump compared to other micropumps include a wide range of possible flow rates, simplicity, constant flow, planar structure, well controlled flow rate, and possible mixing characteristics. The development, fabrication, and testing of the disk pumps are discussed. Flow rates and torque/power requirements are given for various rotational speeds, and the flow patterns through the double-disk pump are described from visualizations made using red Rhodamine dye.

2. Single-disk and double-disk pump configuration and operation

The disk pumps are comprised of one or more spinning disks, a wiper, an inlet channel, and an outlet channel. The two disks of the double-disk pump can be actuated individually, or can be coupled together as seen in Fig. 1. The disk shaft(s) are guided in (a) bearing(s), which also form(s) a seal along the shaft(s) to reduce leakage. The wiper contacts the flat surface of the rotating disk(s), and is the height of the fluid passage. The height of the fluid passage through the pump is the distance between the two disks for the double-disk pump, or the distance between the single disk and the upper wall of the pump for the single-disk pump. The height of the fluid passage through the pump (also the height of the wiper) is referred to as the gap height of the pump. The gap heights used for testing are 78 and 103 μm . The inlet and outlet channel side walls are continuous with the walls of the wiper, as seen in Fig. 2. The fluid flow transitions from a stationary inlet channel to the rotating surface of the disk(s) as the fluid travels from the inlet channel to the pumping volume. The volume of fluid between the two disks or between the single disk and upper pump housing is referred to as the pumping volume.

3. Pump component fabrication

There are five main fabricated components of the viscous disk pump assembly: (i) the disk(s), (ii) top housing, (iii) bottom housing, (iv) bearings, and (v) wiper/channel insert. An exploded view of the double-disk pump is given in Fig. 3. An exploded view of the single-disk pump is identical to Fig. 3 with the exclusion of the top bearing and top disk. In place of the top bearing and top disk, the bottom of the top housing for the single-disk pump is flat and forms the top of the fluid channel through the pump volume as seen in Fig. 1. There are a total of three pump assemblies that are used: (i) the single-disk viscous pump with a disk diameter of 2.38 mm, (ii) the double-disk pump with a disk diameter of 2.38 mm, and (iii) the double-disk pump with a disk diameter of 6.35 mm. The first two pump assemblies, (i) and (ii), are used for flow rate and power testing, and the third pump assembly, (iii), is used for flow visualization testing.

Fabrication of the disk(s) is realized using precision machining techniques. A lathe is used to obtain the desired outside diameter of the disk shaft, and to create the disk surfaces. For the double disk pumps, a hole is bored into one of the disk surfaces, into which the coupling shaft is press-fit. The other disk is machined on the lathe to the desired outside

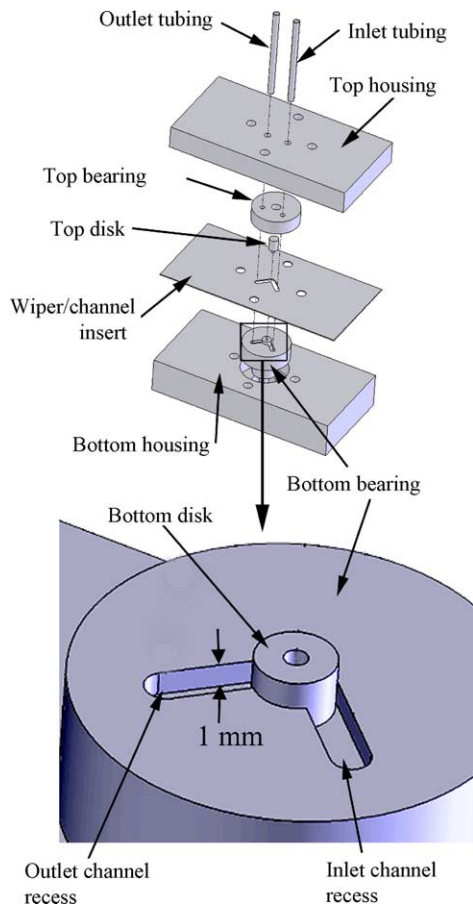


Fig. 3. Exploded view of the double-disk pump assembly.

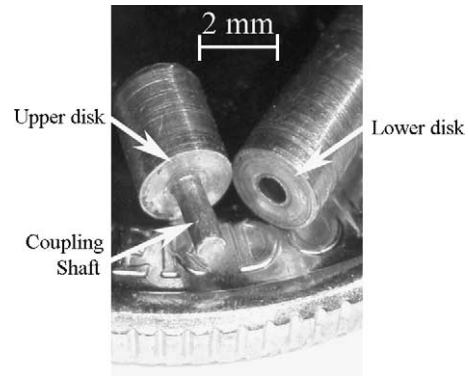


Fig. 4. Double-disk pump shafts before assembly on a United States quarter dollar coin.

diameter and then the coupling shaft is machined on the end, such that the step between the disk shaft diameter and coupling shaft diameter forms the other disk surface as seen in Fig. 4. The coupling shaft is press-fit into the bored hole in one disk until the desired gap height is obtained. The disks for the double-disk pump used for flow rate testing are made from brass with an outer diameter of 2.38 mm. The bottom and upper disks for the double-disk pump used for flow visualization are made from aluminum and acrylic respectively, with an outer diameter of 6.35 mm. The acrylic disk is clear and allows the flow in the pumping volume to be visualized through the disk.

The disk of the single-disk pump is made from type 304 stainless steel. The top housing of all the disk pump assemblies are made from acrylic, to allow the flow passing into and through the pump to be visualized. The top housings have an inlet and outlet passage that connects the inlet and outlet tubing to the inlet and outlet channels of the pump. The top housing of the double-disk pump assembly with the 6.35 mm diameter disks has an ink injection hole that is 0.2 mm in diameter that is located halfway along the inlet channel width, and 3 mm upstream of the pumping volume as seen in Fig. 2. The bottom housing for all pumps is made from aluminum, and contains the lower bearing.

The bearings are made from Torlon 4301 by Solvay Advanced Polymers, a strong plastic with a low coefficient of friction. The upper and lower bearings are press fit into the top and bottom housing, respectively, as shown in Fig. 3. Torlon is used because it has a low coefficient of friction, and can be easily machined. The outer diameter of the bearings is 12.7 mm, and the inner diameter of the bearing is the diameter of the disk shaft. For the single-disk and double-disk assemblies used for flow rate testing, a recess that is 1 mm deep is cut into the bottom bearing under the inlet and outlet channel, as seen in Fig. 3, which increases the cross-sectional area of the fluid passage through the inlet and outlet channel. The expansion of the fluid channel slows the fluid as it enters the recess in the inlet and outlet channels. The slower fluid minimizes losses as the fluid travels to and from the pumping volume. There is no recess in the bottom bearing of

the double-disk pump assembly used for flow visualization testing.

The wiper/channel insert is machined from brass shim stock using a CNC milling machine, and forms the walls of the fluid channels and the wiper. The thicknesses of the brass shim stock used for the flow rate testing and flow visualization testing are 103 and 78 μm , respectively. The widths of the inlet and outlet channels for the flow rate testing and flow visualization testing are 1.19 and 3.18 mm, respectively, or one-half the disk diameter. The wiper/channel insert is positioned between the top and bottom housing. A seal is created around the wiper by tightening bolts that clamp the top and bottom housing together.

4. Experimental apparatus and procedures

The disk pumps are powered by an externally mounted Maxon EC32 number 118891 brushless DC motor that is 32 mm in diameter with an 80 W power rating. The brushless motor is controlled by an Advanced Motion Controls power amplifier (Model #BE12A6). A negative feedback controller is employed to maintain constant speed for any variation in torque. The speed is controlled by adjusting a 15-turn potentiometer. The speed range is 100–13,200 rpm. The motor controller determines the rotational speed from the signal from an optical encoder attached to the motor shaft. This apparatus then produces two voltage signals that are proportional to motor speed and current supplied to the motor, respectively, which are measured using a Keithley 131 Digital Multimeter. Another Keithley 131 Digital Multimeter is used to measure the voltage supplied to the motor at the motor input terminals of the motor controller. The power to the motor is then determined by multiplying the current and voltage supplied to the motor.

The test setup is shown in Fig. 5 and includes a water reservoir, which is large enough that the water level change during operation is negligible. The water tank is connected to the inlet channel by means of inlet tubing. The inlet tubing for the two disk pumps has an inner diameter of 4.5 mm, and length of 381 mm. The outlet channel is connected to

the outlet tubing. The outlet tubing for both disk pumps has an inner diameter of 4.5 mm, and a length of 86 mm. When testing the maximum pressure rise for both pumps, the outlet tubing connects to the bottom of a vertical water column with an inner diameter of 4.5 mm, and height of 300 mm.

The pump assembly is mounted to the base of a linear slide as seen in Fig. 5. The linear slide consists of a stationary base, and a linear sliding “shuttle” that moves relative to the base on linear bearings. The brushless motor and motor coupling shaft are mounted to the shuttle of the linear slide. One end of the motor coupling shaft connects to the motor shaft, and the other end connects to the disk shaft as seen in Fig. 5. The motor coupling shaft is made from aluminum, and is secured by ball bearings at each end. The position of the shuttle, along with the motor and disk shaft, are adjusted and secured using 4–40 positioning bolts. There is one positioning bolt at each of the two ends of the shuttle, such that one positioning bolt is used to adjust the position, and the other is used to immobilize the shuttle. A microscope is used to aid the positioning of the disk by means of the positioning bolts. The microscope is an Infinevar Continually Focusable Microscope (CFM) (0–330 \times magnification), manufactured by Infinity Photo-Optical Co., with a Hitachi HV-C20U-S4 video camera connected to a Sony Tinitron PVM-14N5U high resolution monitor.

Assembly of the double-disk and single-disk pumps starts by connecting the disk pump shaft to the motor coupling shaft on the motor. The bottom housing of the pump is then mounted to a plate that connects to the base of the linear slider as seen in Fig. 5. The position of the disk surface is adjusted so that the disk surface is flush with the top surface of the bottom housing using the positioning bolts. The wiper/channel insert is then positioned and secured in place using two bolts that screw into the bottom housing. Then for the double-disk pump, the coupling shaft with the upper disk is press-fit into the lower disk until the upper disk surface contacts the upper wiper surface. This contact is determined visually with the microscope, and physically by the disks starting to “pull” on the wiper, when the disk is rotated manually. The top housing is then secured, and tightened to minimize leakage. The inlet and outlet tubes are then connected to the top housing.

After assembly and positioning of the disk surface(s) and housing, all the air is bled from the pump assembly using a syringe attached to the end of the inlet tubing. For the dye flow visualization, a 5 ml syringe is filled with dye and connected to the top housing by a clear tube with an outer diameter of 1.58 mm and length of 450 mm. The dye enters the fluid channel through the dye injection hole seen in Fig. 2. This location is the starting point for advection of the dye through the inlet channel then the pumping volume. The clear tube is primed by injecting the dye into the pump housing until dye is seen in the pumping chamber. The pump assembly is then flushed with water, using the syringe attached to the end of the inlet tubing, to clear the dye from the inlet and

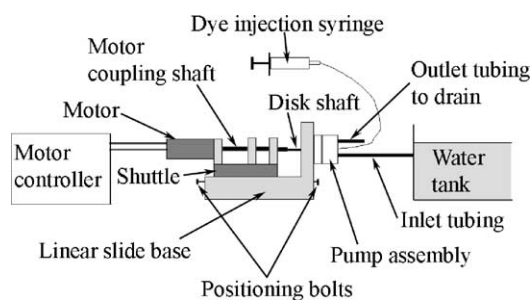


Fig. 5. Experimental testing apparatus. Motor controller has an output signal for shaft speed, and motor current. Dye is injected by tapping on the push rod of the syringe.

outlet channels, and pumping volume. The syringe attached to the end of the inlet tubing is then removed before testing begins.

After these steps are completed, testing is comprised of the following procedures. (1) The system is flushed to ensure there are no air bubbles or trapped particulates in the pumping chamber. (2) The pump motor is activated, and adjusted to produce the desired speed. (3) The pump then continues to operate at constant speed for a minimum period of 20–30 s before testing, so that steady state operation is reached. (4a) For flow rate testing, the timer is started, and water from the outlet tubing is collected. Output signals related to shaft rotational speed and current to the motor are measured and recorded. The power to the motor and the flow rate are then determined and recorded. The flow rate is determined by dividing the amount of water collected by the collection time. (4b) For dye flow visualization, the dye syringe plunger is tapped to inject a small amount of red Rhodamine dye into the fluid flow. Only a small amount of dye is injected into the fluid channel so that minimal disturbance to the fluid in the pumping chamber is caused by the injection of the dye. The movement of the dye is recorded using the Infinivar microscope, mentioned earlier, that outputs to a Matrox video acquisition card in a DELL Workstation 530. The Matrox card records at a rate of 30 frames/s. Due to the frame rate limitations of the Matrox card, disk rotational speed of 211 rpm is used to obtain the flow visualization results. (4c) For the maximum pressure rise testing, water is pumped to the vertical fluid column until the height of the fluid column creates enough backpressure to stop pumping. The vertical distance between the water level at the top of the fluid column and top of the water tank, respectively, is measured to determine the pressure rise using the equation $\Delta P_{\max} = \rho gh$. Where ΔP_{\max} is the maximum pressure rise across the pump, ρ the fluid density, g the gravitational constant, and h is the measured vertical distance. All data are recorded, and then entered and processed using a DELL Latitude laptop computer, and employing Microsoft Excel XP software.

5. Results and discussion

The experimental results are presented in four sections. The first section discusses the operation of the disk pumps. The second section discusses the observed flow patterns in the double-disk pump from the dye flow visualization. The third section discusses flow rate variations and power variations with disk rotational speed for the single-disk and double-disk pumps. The fourth section discusses the overall behavior of the disk pumps relative to other types of micropumps.

5.1. Operation of the disk pumps

Fig. 2 shows three regions within the fluid passage within the pump. The Reynolds number for the tested disk pump are between 3.4 and 64, where the characteristic length is the gap height and the characteristic speed is the outer disk radius multiplied by the disk angular velocity. In region 1, near the inlet, the spinning disk draws fluid away from the inlet wiper face, creating a low static pressure region along the face of the wiper. The resulting pressure gradient induces fluid from the inlet channel into the pump entrance, along the face of the wiper. Fig. 2 then shows that fluid is forced circumferentially through region 2 due to the viscous forces applied to the fluid by the spinning disk(s). The fluid circumferential velocity decreases as the fluid approaches the wiper near the outlet in region 3, where static pressure increases locally. The resulting static pressure then forces fluid toward the outlet channel, motion which is assisted by centrifugal forces at higher disk rotational speeds.

5.2. Dye flow visualization for the double-disk pump

The arrangement of the flow channels, disks, and wiper is shown in Fig. 6. The images of the dye moving through the pumping volume are digitally enhanced using Adobe Photoshop 7.0 so the red dye can be readily seen in a grey-scale format. This is accomplished by outlining and selecting the

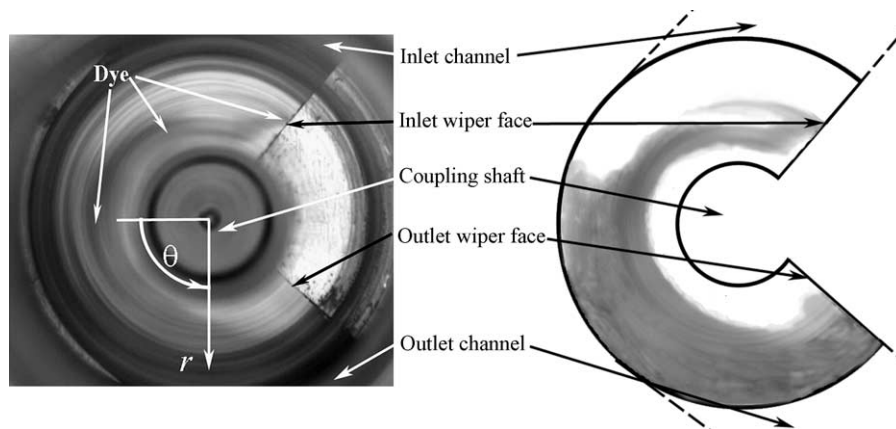


Fig. 6. Configuration of the double disk pump for dye flow visualization. The view looks down through the top disk, into the pumping volume. The image on the right is digitally enhanced to show a grey-scale distribution of the dye arrangement.

region containing red dye, and removing the remainder of the unselected image. The region containing red dye is then superimposed on the outline of the pumping volume shown on the right side of Fig. 6. Streaks due to particulate on the disk surface and other non-dye objects are then removed by blending the surrounding red dye through the streaks or objects. The fluid and dye enter into the pumping volume through the inlet channel, and exit through the outlet channel. For the data presented, the disks are rotating counter-clockwise at a rotational speed of 211 rpm, with a gap height of 78 μm . The inner and outer disk diameters are 1.9 and 6.35 mm respectively, as mentioned.

Fig. 7 contains eight frames that show the progression of the dye through the pumping volume. A radial black line shows the position of the disks as they rotate. Sequential frames 1–2, and 5–8 are separated by 0.095 s, and sequential frames 2–5 are separated by 0.063 s. Frames 1–8 show two complete revolutions of the disks. The three physical effects, which affect fluid motion through the pumping volume, are viscous forces due to the spinning of the disks, static pressure variations, and centrifugal forces acting on the fluid. The centrifugal forces generally force the fluid radially outward, but are insignificant at small Reynolds numbers. The viscous forces are largest near the disk surfaces and generally induce the flow to move in a circumferential direction. The curvature of the streamlines within the pump volume results in an inviscid static pressure increase with radius. This pressure gradient then tends to induce fluid motion from larger to smaller radii. The regions labeled in Fig. 2 are used to discuss the fluid flow and dye distributions in Fig. 7 as they are affected by the relative magnitudes of these physical effects.

Referring to the data in Fig. 7, some of the dye enters the pumping volume just prior to frame 1 and continues to enter the pumping volume during the time intervals associated with frames 1–3. The entering dye close to the disk surfaces then moves circumferentially, due to viscous forces from the disks. Some of the dye midway between the disks at larger radii moves circumferentially due to the viscous forces, but at a slower rate than the dye near the disk surface at the same radial and circumferential locations. Some of the dye midway between the disks in region 1 (shown in Fig. 2) is advected to smaller radii toward the coupling shaft toward a region of lower static pressure. As this center dye moves to smaller radii, some of the dye is advected in the z -direction to the disk surface and then moves circumferentially, which is evident from larger amounts of dye moving circumferentially in frames 1–3. The z -direction is perpendicular to the disk surfaces as shown in Fig. 1. Because the dominant pressure forces in region 1 (which act in an inviscid manner) generally induce motion to smaller radii, they tend to force fluid into the pumping volume, whereas the viscous forces move the fluid through the pumping volume.

Frames 2 and 3 of Fig. 7 show that the largest portions of the dye in region 2 move circumferentially as a result of viscous forces. This motion occurs as dye continues to enter the pumping volume from the inlet channel. Some motion of

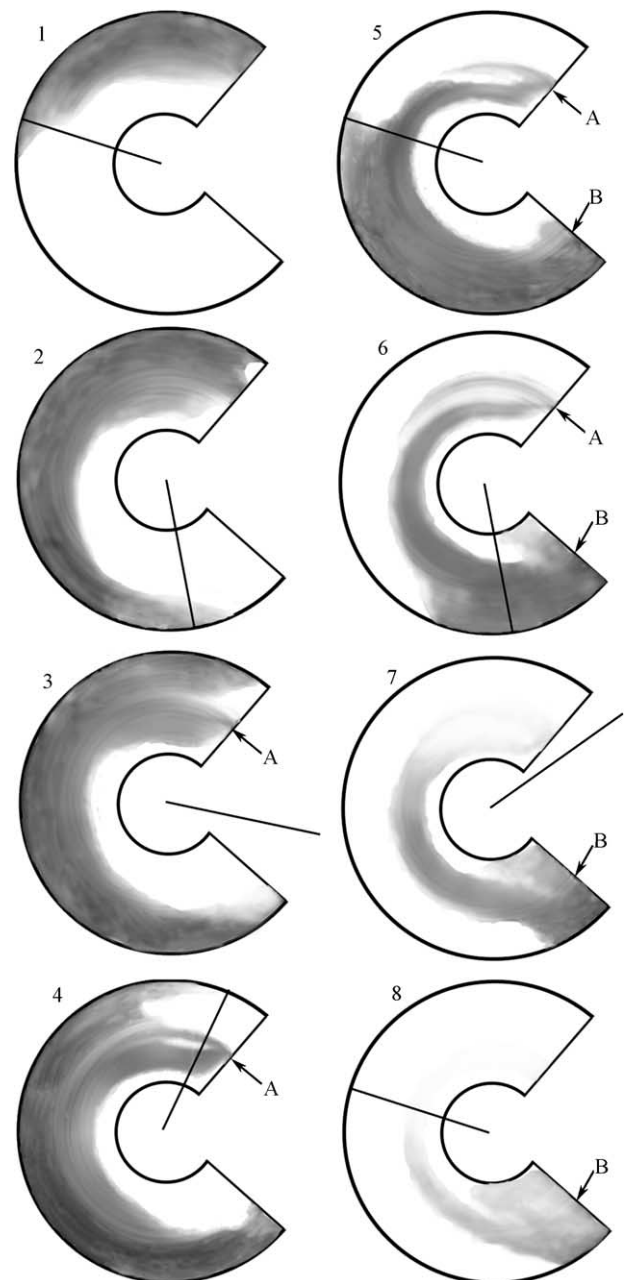


Fig. 7. Rhodamine dye moving through the pumping region of the double disk viscous pump through three complete disk revolutions. Disks are spinning counter-clockwise with a rotational speed = 211 rpm, a disk diameter = 6.35 mm, and a gap height = 78 μm . The black line is inserted to show the rotation of the disk. Sequential frames 1–2 and 5–8 are separated by 0.095 s, and sequential frames 2–5 are separated by 0.063 s. Locations A and B are stagnation points.

dye to smaller radii is also apparent through the pump volume in frames 2–4 as a result of diffusion and advection induced by the radial pressure gradient.

A circumferential pressure gradient is also present in the pump volume mostly because of interactions between the pump fluid and the wiper. This gives a static pressure rise with circumferential position through the pump volume, such

that a region of lower static pressure is present near the inlet wiper face, and a region of higher static pressure is present near the outlet wiper face. This static pressure variation then opposes the motion induced by rotation and viscous forces. At larger radii, the magnitude of the viscous forces over the height of the channel are greater than the opposing circumferential pressure forces, which results in flow through the pumping volume from the inlet to the outlet of the pump. At smaller radii in region 2, where the viscous forces are the smallest, the opposing circumferential static pressure variation causes some of the fluid midway between the disks to move opposite the main flow direction, or the direction of the rotating disks, resulting in a recirculating flow at smaller radii. This recirculating flow is discussed in additional detail below.

The circumferential static pressure variation forces some of the dye midway between the disks in region 1 (shown in Fig. 2) at smaller radii to move toward the inlet wiper face and stagnate at a position about halfway along the inlet wiper face. This stagnation is evident in frames 3–6 and is labeled “A” in Fig. 7. The stagnation of the dye along the inlet wiper face provides evidence of the location of the minimum static pressure, and is located midway between the two rotating disks. Fluid moves toward this stagnation point radially from larger radii, due to the radial pressure gradient. Fluid also moves toward the stagnation point radially, from smaller radii, and circumferentially, opposite the main flow direction, due to the recirculating flow. Frames 4–7 also show that some of the dye near the stagnation point is then advected in the z -direction toward the disk surfaces resulting in the circumferential motion of the dye away from the stagnation point.

The flow midway between the disks in region 2 (shown in Fig. 2) at smaller radii is in a circumferential direction which is opposite to the direction of the disk rotation. Additional evidence of this recirculating flow is shown in frames 5–8 by the movement of some of the dye from outlet wiper face toward the coupling shaft and eventually toward the inlet wiper face. The fluid flow midway between the disks in region 2 at larger radii is in the main flow direction in a “positive” circumferential direction. As a result, the circumferential velocity of the fluid is very small at locations in between these inner and outer radii regions, midway between the disks, in region 2. The radial position for which the circumferential velocity becomes very small is evident in frames 5–7 at a radial location about 1/3 the distance between the inner and outer radii of the pumping volume (in region 2). The circumferential velocity of the dye is then “negative” at smaller radii, and “positive” at larger radii (relative to the rotation direction of the disks). Some of the dye that is advected or diffused in the z -direction toward the disk surface where it then moves circumferentially toward the outlet wiper face, which results in the eventual movement of the dye toward the outlet channel, as seen in frame 8.

Another stagnation point also exists in region 3 near the outlet wiper face at a location of highest static pressure, and

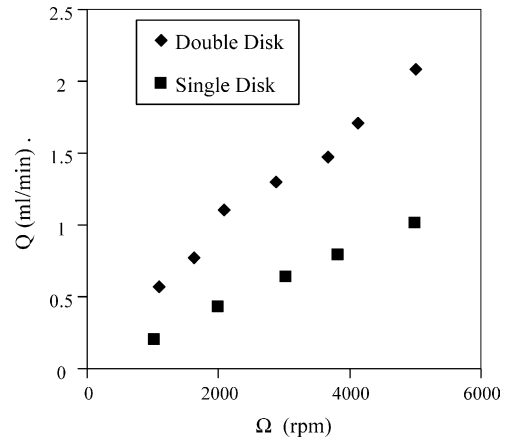


Fig. 8. Flow rates and rotational speeds for the disk pumps from experimental testing. Disk diameter = 2.38 mm, gap height = 103 μ m.

is labeled “B” in Fig. 7. Near this point, the fluid is forced either (i) toward the outlet channel, or (ii) toward the coupling shaft (recirculating flow). Evidence of this stagnation point is seen in frames 5–8 as the dye interacts with the outlet wiper face. Near this location, some dye moves toward the outlet because of centrifugal forces and local pressure gradients, and some dye moves in the radial direction toward the coupling shaft because of local pressure gradients in region 3.

The overall results of the observed flow patterns in Fig. 7 indicate a net flow through the pumping volume.

5.3. Flow rate variations and pressure rise variations with disk rotational speed for the single-disk and double-disk pumps

Flow rate variations for the single-disk and double-disk pumps are given in Fig. 8, for rotational speeds ranging from 1000 to 5000 rpm, a disk diameter of 2.38 mm, and a gap height of 103 μ m. The uncertainty magnitudes for the flow rate and rotational speed in Fig. 8 are approximately $\pm 3\%$ and $\pm 4\%$, respectively. The results in Fig. 8 show that flow rates increase nearly linearly with rotational speed for both types of pumps. This linearity provides additional evidence of the dominating influences of the viscous forces induced by disk rotation. For a rotational speed of 5000 rpm, the maximum flow rates for the single-disk pump and double-disk pump are achieved, and are 1.0 and 2.1 ml/min, respectively. Even higher flow rates can be obtained with greater rotational speeds, and larger disk diameters. Note also that flow direction can be reversed by changing the rotational direction of the disk(s).

Maximum pressure rise variations for the single-disk and double-disk pumps are given in Fig. 9 for rotational speed ranging from 1000 to 5000 rpm, a disk diameter of 2.38 mm, a gap height of 103 μ m, and a flow rate of zero. The uncertainty magnitudes for the flow rate and rotational speed in Fig. 9 are approximately $\pm 3\%$ and $\pm 4\%$, respectively. The maximum

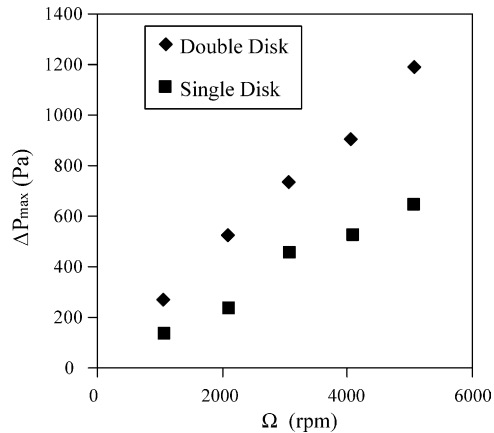


Fig. 9. Maximum pressure rises and rotational speeds for the disk pumps from experimental testing. Disk diameter = 2.38 mm, gap height = 103 μm .

pressure rise for the single-disk and double-disk pumps is 643 Pa and 1.19 kPa, respectively. The maximum pressure rise increases nearly linearly with increasing rotational speed for both disk pumps. Even higher flow rates can be obtained at greater rotational speeds.

No leaks are observed from the disk pump assembly during flow rate testing. During testing of the maximum pressure rise, a leak on the order of 1 $\mu\text{l}/\text{min}$ is observed between the stationary bottom bearing and rotating bottom disk shaft due to the higher pressure conditions inside the pumping chamber. The observed leakage may be reduced by changing the bearing design, or pump configuration.

Fig. 10 shows the power supplied to the motor as it varies with rotational speed for the double-disk pump with disk diameter of 2.38 mm. The first set of data shows the power supplied to the motor before the motor is attached to the motor coupling shaft. The second set of data shows the power supplied to the motor during testing. The motor used for testing is chosen to demonstrate the operation of the disk pumps; however, smaller motors can be used instead. The power requirements can also be lowered further by optimizing the bearing design.

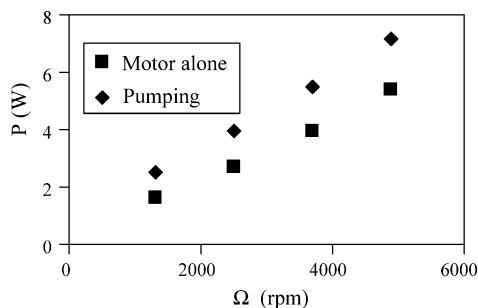


Fig. 10. Variation of power supplied to the motor with rotational speed for the double-disk viscous micropump. The first data set is the power to the motor before connection to motor shaft to the motor coupling shaft, and the second set of data is the power during pumping. Disk diameter = 2.38 mm, gap height = 103 μm .

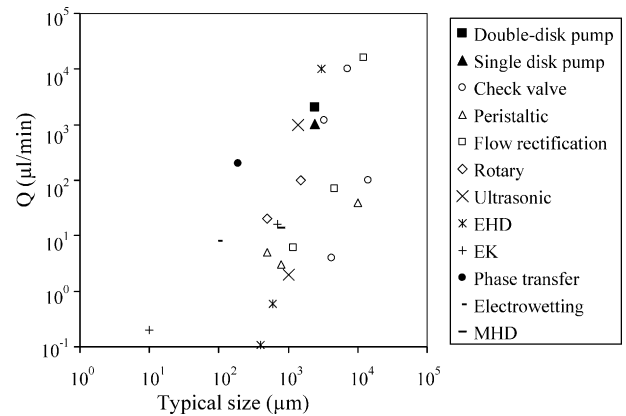


Fig. 11. Maximum flow rate and typical size of the single-disk pump, double-disk pump, and other micropumps. Typical size is defined by the disk diameter, diaphragm diameter, or pumping channel width. The size of the pump actuator is not included in the typical size [2–13,17–26].

5.4. Overall behavior of the disk pumps relative to other types of micropumps

The maximum flow rates and typical size of the single-disk pump, and the double-disk pump compared to other micropumps are shown in Fig. 11. The size of the disk pumps is based on the disk diameter. Typical sizes for the check-valve pumps, peristaltic valves, flow rectification pumps, and rotary pump are based on pump chamber diameters. Typical sizes for all other pumps are based upon the channel width. Note that the typical size does not include the actuator of the disk pumps, or the other micropumps. Fig. 10 shows that the flow rates for the single-disk and double-disk pumps are larger than values for many other micropumps, with typical sizes falling in the middle of the range of values for the micro-pumps considered [2–13,17–26].

6. Summary and conclusions

Two versions of a novel pump called the single-disk viscous pump and double-disk viscous pump are developed and tested. The advantages of this micropump compared to other micropumps include a wide range of possible flow rates, simplicity, steady flow with time, planar structure, well controlled flow rate, and if desired, ability to augment mixing in the flow. The experimentally measured flow rate shows an increase with rotational speed that is nearly linear, which provides evidence of the dominating influences of the viscous forces induced by the rotating disks. The fluid pumping direction can be reversed by changing the rotational direction of the disk(s). The design of the disk pumps is simple, and can potentially be fabricated using microfabrication technology due to the planar structure of the pump. Dye inserted into the pumping volume shows flow movement due to pressure gradients, viscous forces, and centrifugal forces. The movement of the dye through the pump also provides evidence of enhanced mixing as it is advected and diffused through

the pump volume. Potential applications for the disk pumps include transport of biomedical fluids, drug delivery, total analysis systems, and electronics cooling.

Acknowledgments

Work presented in this paper was supported by the National Science Foundation (NSF) through the IGERT Program, grant number DGE 9987616.

References

- [1] N.T. Nguyen, S.T. Wereley, *Fundamentals and Applications of Microfluidics*, Artech House Inc., Norwood, 2002, pp. 292–337.
- [2] A. Olsson, G. Stemme, E. Stemme, A valve-less planar fluid pump with two pump chambers, *Sens. Actuators A* 47 (2) (1995) 549–556.
- [3] J.H. Tsia, L. Lin, A thermal bubble actuated micro nozzle-diffuser pump, *J. MEMS* 11 (2002) 665–671.
- [4] N.T. Nguyen, X.Y. Huang, Miniature valveless pumps based on printed circuit board technique, *Sens. Actuators A* 88 (2) (2001) 104–111.
- [5] E. Meng, X.-Q. Wang, H. Jak, Y.-C. Tai, A check-valved silicone diaphragm pump, in: *Proceedings of the MEMS '00, 13th International Workshop Micro ElectroMechanical Systems*, Japan, January 23–27, 2000, pp. 23–27.
- [6] W.L. Benard, H. Kahn, A.H. Heuer, M.S. Huff, Thin film shape-memory alloy actuated micropumps, *J. MEMS* 7 (2) (1998) 245–251.
- [7] V. Gass, G.H. Van der Schoot, S. Jeanneret, N.F. DeRooij, Integrated flow-regulated silicon micropump, *Sens. Actuators A* 43 (1994) 335–338.
- [8] H.Q. Li, D.C. Roberts, J.L. Steyn, K.T. Turner, J.A. Carretero, O. Yaglioglu, Y.-H. Su, L. Saggere, N.W. Hagood, S.M. Spearing, M.A. Schmidt, R. Mlcak, K. Breuer, A high frequency high flow rate piezoelectrically driven MEMS micropump, in: *IEEE Solid State Sensors and Actuators Workshop*, Tech Digest, Hilton Head SC, 2000, June, 2000, pp. 69–72.
- [9] A. Richter, A. Plettner, K.A. Hofmann, H. Sandmaier, A micro-machined electrohydrodynamic (EHD) pump, *Sens. Actuators A* 29 (1991) 159–168.
- [10] S.F. Bart, L.S. Tavrow, M. Mehregany, J.H. Lang, Microfabricated electrohydrodynamic pumps, *Sens. Actuators A* 21–23 (1990) 193–198.
- [11] S.H. Ahn, Y.K. Kim, Fabrication and experiment of a planar micro ion drag pump, *Sens. Actuators A* 70 (1998) 1–5.
- [12] A. Furuya, F. Shimokawa, T. Matsuura, R. Sawada, Fabrication of fluorinated polyimide microgrids using magnetically controlled reactive ion etching (MC-RIE) and Their applications to a ion drag integrated micropump, *J. Micromech. Microeng.* 6 (1996) 310–319.
- [13] S. Zeng, C.H. Chen, J.C. Mikkelsen, J.G. Santiago, Fabrication and characterization of electrokinetic micro pumps, in: *Proceedings of the Seventh Intersociety Conference on Thermal and Thermomechanical Phenomena in Electronic Systems*, vol. 2, CPMT/IEEE, Las Vegas, May, 2000, pp. 31–36.
- [14] C. Hainan, Z. Ahaoying, L. Yong, Y. Xiongying, Y. Yihua, A novel centrifugal miniature pump and its medical application, in: *Proceedings of the 1997 International Symposium on Micromechatronics and Human Science*, IEEE, October, 1997, pp. 115–117.
- [15] M. Kilani, P. Galambos, Y. Haik, C.J. Chen, Design and analysis of a surface micromachined spiral-channel viscous pump, *J. Fluids Eng.* 125 (2) (2003) 339–344.
- [16] M. Sen, D. Wajerski, M. Gad-El-Hak, A novel pump for MEMS applications, *J. Fluids Eng.* 118 (3) (1996) 624–627.
- [17] C.H. Ahn, M.G. Allen, Fluid micropumps based on rotary magnetic actuators, in: *Proceedings of the MEMS 1995*, January–February, 1995, pp. 408–418.
- [18] J. Dopfer, M. Clemens, W. Ehrfeld, S. Jung, K.-P. Kamper, H. Lehr, Micro gear pumps for dosing of viscous fluids, *J. Micromech. Microeng.* 7 (2) (1997) 230–232.
- [19] H. Mizoguchi, M. Ando, T. Mizuno, T. Takagi, N. Nakajima, Design and fabrication of light driven micropump, in: *Proceedings of the MEMS 92, Fifth IEEE International Workshop MEMS*, Germany, January 25–28, 1992, pp. 31–36.
- [20] C. Grosjean, Y.C. Tai, A thermopneumatic peristaltic micropump, in: *Proceedings of the Transducer '99, the 10th International Conference on Solid State Sensors and Actuators*, June 7–10, 1999, pp. 1776–1779.
- [21] C. Cabuz, W.R. Herb, E.I. Cabuz, S.T. Lu, The dual diaphragm pump, in: *Proceedings of the MEMS '01, 14th IEEE International Workshop MEMS*, Switzerland, January 21–25, 2001, pp. 519–522.
- [22] R.M. Moroney, R.M. White, R.T. Howe, Ultrasonically induced microtransport, in: *Proceedings of the MEMS '1, Fourth International Workshop MEMS*, Japan, January 30–February 4, 1991, pp. 277–282.
- [23] S. Miyazaki, T. Kawai, M. Araragi, A Piezoelectric Pump Driven by a Flexural Progressive Wave, in: *Proceedings of the MEMS '1, Fourth International Workshop MEMS*, Japan, January 30–February 4, 1991, pp. 283–288.
- [24] H. Takagi, R. Maeda, K. Ozaki, M. Parameswaran, M. Mehta, Phase transformation type micropump, in: *Proceedings of the International Symposium on Micro Machine and Human Sciences*, Japan, October, 1994, pp. 199–202.
- [25] H. Matsumoto, J.E. Colgate, Preliminary investigation of micropumping based on electrical control of interfacial tension, in: *Proceedings of the MEMS '90, Second IEEE Workshop of MEMS*, CA, February 11–14, 1990, pp. 105–110.
- [26] A. Hatch, A.E. Kamholz, G. Holman, P. Yager, K.F. Bohringer, A ferrofluidic magnetic micropump, *J. MEMS* 10 (2) (2001) 215–221.
- [27] G.E. Karniadakis, A. Beskok, *Micro flows fundamentals and simulation*, Springer, New York, 2002, pp. 1–31.
- [28] D. Blanchard, P. Ligrani, B. Gale, Viscous Micropump, Provisional Patent: University of Utah Attorney Docket Number U2550P2, 2003.
- [29] D. Blanchard, P. Ligrani, B. Gale, “Rotary Centrifugal and viscous micropumps”, US Patent Office, Application No. PCT/US2004/028890, September 3 Patent applied for (2004).

Biographies

Danny Blanchard received a Bachelor of Science degree in Mechanical Engineering from the University of Utah in 2001. At present he is a PhD student in Mechanical Engineering at the University of Utah, studying fluid physics in micro-pumps and micro-systems. Danny has been the recipient of the Wayne Brown Fellowship, and funding from the National Science Foundation (NSF) through the IGERT Program.

Phil Ligrani is currently Professor of Mechanical Engineering, and Director of the Convective Heat Transfer Laboratory in the Department of Mechanical Engineering at the University of Utah. Current research areas include sensor and measurement techniques, convective heat transfer, heat transfer augmentation, internal cooling, turbulent boundary layers, transitional phenomena, film cooling, macro-scale and micro-scale pumping systems, and peptide suspension flows. He is currently Associate Editors for the *Journal of Heat Transfer* and the *Journal of Fluids Engineering*. Honors and awards include “Professor of the Year”, ASME Fellow, an SCIES-AGTSR Faculty Fellowship, Universitaet Karlsruhe Guest Professorship, a NASA Space

Act Tech Brief Award, and the Carl E. and Jessie W. Menneken Faculty Award for Excellence in Scientific Research. His website is: <http://www.mech.utah.edu/PEOPLE/faculty/ligrani/ligraniFrameset.htm>.

Bruce K. Gale received his B.S. in Mechanical Engineering from Brigham Young University in 1995 and a PhD in Bioengineering from the University of Utah in 1999. He spent over two years as an Assis-

tant Professor of Biomedical Engineering at Louisiana Tech University and the Institute for Micromanufacturing. In December of 2001 he joined the Mechanical Engineering Department at the University of Utah as an Assistant Professor. His interests include medical and biological based applications of microfluidics and his work has recently involved micro-machined particle separation systems and detectors, microarray manufacturing methods, and sensors related to these applications.